Astron. Astrophys. 319, 683–693 (1997)

ASTRONOMY
AND
ASTROPHYSICS

Cycle 19 facula dynamics

II. Meridional circulation, rms velocity, and Reynolds stresses

N. Meunier[1], **E. Nesme-Ribes**[1], **and B. Collin**[2]

[1] URA 2080 CNRS, Département d'Astronomie Solaire et Planétaire, Observatoire de Paris, 5 Place Janssen, F-92195 Meudon, France
[2] CREA/SP, Etablissement Technique Central de l'Armement, F-94114 Arcueil, France

Received 20 May 1996 / Accepted 14 August 1996

Abstract. We investigated the meridional circulation of photospheric faculae throughout cycle 19. Together with the rotation observed in a companion paper (Meunier et al. 1996), we were able to address the problem of the existence of the observed differential rotation. The meridional circulation is characterized by a strong north-south asymmetry. The distribution of meridional circulation around the mean value confirms the existence of two populations detected in Meunier et al. (1996). An investigation of the rms velocities yields information on the variation of the anisotropy between the two horizontal motions and the latitudinal dependence of the small-scale kinetic energy. Lastly, a very small facula covariance has been measured, and its variation during the cycle has been established.

Key words: Sun: faculae – Sun: magnetic fields – Sun: rotation – sunspots – Turbulence

1. Introduction

The only systematic analysis of facula dynamics to date was developed by Belvedere et al. (1976). Faculae observed by Belvedere et al. were obtained in a rather broad bandwidth around the Ca II K line, and thus are formed at the chromospheric level (Godoli 1969). These authors measured east-west motions of facula barycenters as well as their meridional drifts, and from this calculated the correlation between horizontal motions, i.e. the covariance, which is a measure of the Reynolds forces at work. They found a covariance ranging from 10^7 to $4\ 10^7$ cm^2/s^2, which was consistent with an angular momentum transport via Reynolds stresses, contributing to maintaining the differential rotation. Schröter & Wöhl (1976) observed the proper motion component of Ca^+-network fine mottles, also formed in the chromosphere. They found a significant positive covariance ($4\ 10^7$ cm^2/s^2) close to the one measured by Belvedere et al. (1976).

Send offprint requests to: N. Meunier

Cycle 21 small-scale magnetic fields (corresponding to the photospheric level) have also been studied, by Komm et al. (1993; 1994). They obtained a poleward meridional flow of the order of 10 m/s, with a maximum at mid-latitudes. At latitudes between 15° and 45°, the amplitude was about 25% higher at cycle minimum than at the maximum. They observed no strong north-south asymmetry. Komm et al. (1984) calculated a very small covariance.

In this paper, we will address certain aspects of photospheric facular point dynamics, on the basis of the Meudon K_{1v} spectroheliograms, revealing the photospheric level about 500 km above the solar surface. These Meudon faculae are similar to the bright elements seen on Kitt Peak magnetograms, so the comparison should be more straightforward than with the sample of Belvedere et al. (1976). However, the comparison with chromospheric faculae is not entirely irrelevant, because it shows the heightwise spatial variation of the rotation and meridional circulation. In our study, we selected cycle 19 faculae over the time interval 1957 to 1964, as this period was the most active of the last four centuries. We also established comparisons between facula properties with those of sunspots, deduced from the same images, because the two tracers give complementary results: faculae cover a wider surface of the solar disk, whereas sunspots are more deeply anchored so that the two tracers give complementary results. Cycle 19 sunspots have been studied in Nesme-Ribes et al. (1996b).

Observational data and tracking procedures are described in Sect. 2. Various error sources are listed in Sect. 3. In Sect. 4, we investigate facula meridional circulation (denoted "m.c." hereafter), which is related to the differential rotation (Meunier et al. 1996, referred to hereafter as Paper I) and its origin. The m.c. might even play a direct role in the solar dynamo, as shown by Choudhuri et al. (1995). That is, if dynamo waves progress towards the poles when there is no m.c., a reasonable m.c. could reverse this propagation. We investigate facula m.c. in Sect. 4.

The rms velocities are also quite pertinent. There is a hierarchy of convective motions, which contribute to the rms velocity (for both m.c. and angular rotation). Some of their properties can be induced from variations in rms velocities of magnetic

tracers during cycle 19. Our prime motivation in this study is to find the dependence of the degree of anisotropy (between the two horizontal motions) on cycle phase and latitude. An interpretation in terms of turbulent kinetic energy should also yield important clues to the behavior of the energy contained in the small-scale convective eddies (Canuto et al. 1994). This question is explored in Sect. 5.

One hotly debated issue is the origin of the differential rotation, which is a key ingredient in solar dynamo theory. Theories of differential rotation are built on the angular momentum conservation equation (see Stix 1989, among others). This equation contains two terms: axisymmetric (i.e. turbulent convection) and non-axisymmetric (i.e. global convection).

Certain axisymmetric models require a convective latitude-dependent heat flux, and thereby a pole-equator temperature difference, in order to generate differential rotation. This implies the existence of m.c. Other approaches also require anisotropic viscosity (higher viscosity in the horizontal direction). Both models explicitly calculate the m.c. and angular velocity only.

In non-axisymmetric models, a number of correlations appear between latitudinal and longitudinal motions, due to the interaction between global Coriolis force and non-axisymmetric motions (convective cells). These correlations represent the angular momentum transport by the Reynolds stresses: the smaller the Rossby number $Ro = u/(2\Omega l)$ (where u is a typical velocity in the non-axisymmetric eddies, l a typical cell size, and Ω the angular velocity), the more efficient this interaction. So the process is more efficient with supergranulation than with granulation. The giant meridional cells should also be more efficient than supergranulation. Rüdiger (1977) showed that Reynolds stresses contain a diffusive term (which must be positive in order to transport angular momentum equatorward) and also a non-diffusive term, the Λ-effect, which may be of either sign for equatorward transport. As we observe both terms at the same time, the interpretation of the observed covariance sign is not straightforward. In Sect. 6, we derive facula covariance versus latitude, and also the latitude-averaged covariance over each hemisphere.

2. Observational data and tracking procedure

Our observational data and tracking procedures were described at length in Paper I and in Collin et al. (1995). Briefly, the facular bright point meridional motions are inferred from Meudon K_{1v} spectroheliograms (1.5 Å off the Ca II K line center) reflecting the photospheric level about 500 km above the $\tau = 1$ level (Nesme-Ribes et al. 1996a). The images have been digitized with 1.8 arcsecond resolution. We selected the time interval 1957 to 1964, during which 47434 points were detected (Paper I).

3. Sources of error

Paper I discussed the existence of a small bias in the angular velocity that was detected in the form of an east-west asymmetry (angular velocity versus disk longitude). The slope of the bias (m. c. versus disk longitude) is very small - an order of magnitude smaller than the rotation bias -, so that we can neglect it in the present paper. Random errors on individual points m.c. are similar to the ones given in Paper I for the angular rotation, i.e. 15 m/s at the disk center.

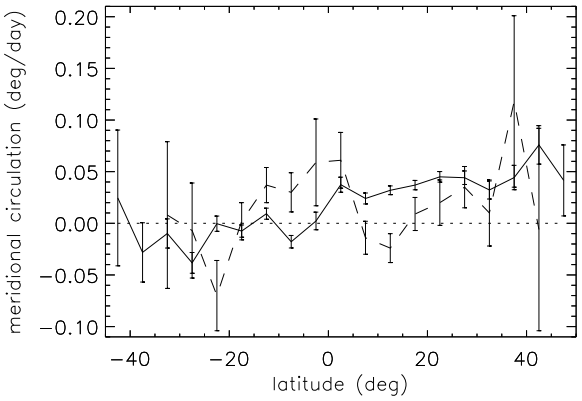

Fig. 1. Meridional circulation for faculae in [1957-1964] (solid line) and sunspots in [1957-1962] (dashed line). Values are given in degrees/day. Error bars are at the 1-σ confidence level

4. Meridional circulation

4.1. Results

Fig. 1 shows m.c. averaged in 5° latitude bins for the whole data set. We adopt the following convention: a positive m. c. indicates a motion towards the pole in the northern hemisphere and towards the equator in the southern. Error bars are at the 1-σ confidence level. At cycle maximum, faculae reach latitudes of up to 50°. A strong north-south asymmetry of m.c. is observed in Fig. 1. The southern hemisphere shows a negligible motion while a significant northward circulation, of up to about 0.05°/day (7 m/s), occurs in the northern hemisphere. Such a north-south asymmetry was not observed by Komm et al. (1993), in their study of small-scale magnetic field dynamics. This north-south asymmetry of m.c. was present, though, in cycle 19 facula rotation rates (Paper I).

Table 1 and Fig. 2 show the yearly latitude-averaged m.c. computed for each hemisphere. The southern m.c. is small and hardly significant during the whole cycle. But the northern m.c. shows a significant variation: from its maximum at cycle maximum, it decreases to very small values at cycle minimum. This is in clear disagreement with the results of Komm et al. (1993), who found a faster meridional flow at the minimum of the solar cycle, though for an other cycle.

4.2. Comparison with cycle 19 sunspots

Sunspots have been studied in Nesme-Ribes et al. (1996b) for the same time interval from 1957 to 1962. Sunspot m.c. is shown in Fig. 1. They exhibit an equatorward motion at low latitudes and a poleward motion at high latitudes. This sunspot m.c. pattern has already been observed for cycle 21 sunspots (Ribes &

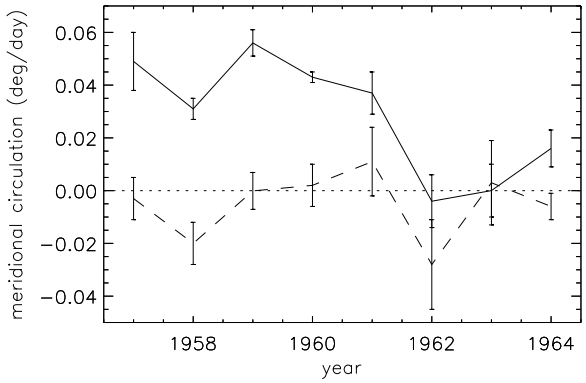

Fig. 2. Variation of facula meridional circulation in [1957-1964] in each hemisphere (solid line: northern hemisphere; dashed line: southern hemisphere). Values are given in degrees/day. Error bars are at the 1-σ confidence level

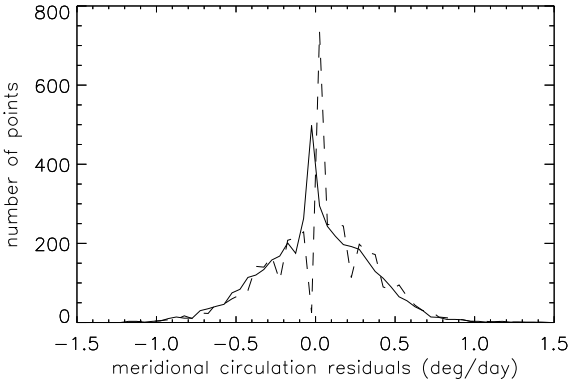

Fig. 3. Histogram showing the distribution of 1959 facula meridional circulation (bin=0.05°/day) around the mean (solid line) and around zero value (dashed line)

Table 1. Facula meridional circulation averaged in each hemisphere (in degrees/day). Error bars are at the 1-σ confidence level

year	North m.c.	South m.c.
1957	0.049±0.011	-0.003±0.008
1958	0.031±0.004	-0.020±0.008
1959	0.056±0.005	-1.10^{4}±0.007
1960	0.043±0.002	0.002±0.008
1961	0.037±0.008	0.011±0.013
1962	-0.004±0.010	-0.028±0.017
1963	3.10^{-5}±0.010	-0.013±0.021
1964	0.016±0.007	0.003±0.016
1957-1964	0.036±0.003	-0.006±0.005
1957-1960	0.045±0.002	-0.007±0.004
1961-1964	0.016±0.004	-5.10^{-4}±0.012

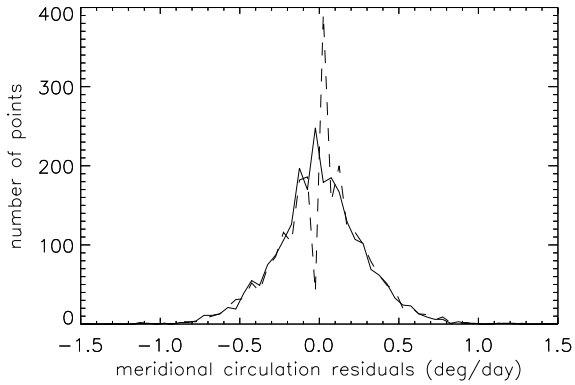

Fig. 4. Histogram showing the distribution for cycle 19 sunspot meridional circulation (bin=0.05°/day) around the mean (solid line) and around zero value (dashed line)

Bonnefond 1990, Nesme-Ribes et al. 1993b). The differences observed between sunspot and facula dynamics are possibly due to the anchorage depth of the two tracers. This is in agreement with the very different rotational properties of sunspots and faculae already observed in Paper I.

4.3. Faculae meridional circulation distribution

Paper I mentions the presence of a large dispersion around the mean rotation rate, in which we detected a shape-asymmetry of the rotation distribution with respect to the mean. Here, we will now look to see whether the facula m.c. has similar shape-asymmetry.

The m.c. histogram shows a strong and sharp peak close to the m.c. value of zero (Fig. 3). The mean value is close to zero. We observe dips in the histograms, especially for the distribution around zero. These are due to the tracking procedure: considering the spatial resolution, the dips depend on the bin size used to build the histogram. These dips were not observed for angular rotation (Paper I) because the differential rotation mixed them.

However, the shape is far from gaussian, and a sharp and strong peak is observed near the zero value. We recall that Paper I distinguished two populations: one (I) with a high rms velocity and an average rotation rate close to that of the whole set; and another one (II) with a low rms velocity and a lower rotation rate. The present peak is probably associated with population II. So population II rms m.c. appears to be very small.

To determine the m.c. properties of population II, we selected points from this population using a two-gaussian fit on the angular velocity histogram per latitude bin. We investigate the particular case of 1959 in the latitude range [5°N-20°N] (Paper I).

We obtain the following result. The restricted set contains a higher percentage (64 %) of points with a zero meridional circulation values than the whole set (29 %). The restricted set m.c. is two times smaller than the whole set m.c., and about 10% of the whole set belongs to population II, compared to 50% in the case of the restricted set. So we estimate population II m.c. to be one order of magnitude smaller than population I m.c.

4.4. Histogram asymmetry of sunspot meridional circulation

A similar histogram for sunspot m.c. shows the same dips but no strong shape-asymmetry (Fig. 4). So if two populations do exist (as detected from their angular velocity in Paper I), their rms velocities as well as their m.c. are very similar. A two-gaussian fit shows that the fastest population (I) has a higher m.c. (by 0.04°/day) than population II. The m.c. is positive for population I and negative for population II.

4.5. Polar field reversal

Facula m.c. is stronger towards the north pole in the northern hemisphere. Furthermore, we observe some activity at higher latitudes (Paper I) in the northern hemisphere. So, from the Leighton's model (1969), which assumes that polar reversal is due to the slow poleward migration of magnetic fields, we expect an earlier polar field reversal in the northern hemisphere. Both Babcock (1959) and Sheeley (1976) noted that the south pole reversal occurred before the North (respectively mid-1957 and end of 1958). However, Makarov (1984) found that the situation is more complex, sometimes observing a three-fold inversion of the polar magnetic field in one hemisphere. This was precisely the case for the northern hemisphere during cycle 19: the first reversal occurred at the beginning of 1958 for the latitude +90° and at the end of 1958 for -90°. So our higher meridional circulation in the North, and this observed time reversal, are consistent with the Leighton's picture for the poloidal magnetic field reversal.

5. Small-scale kinetic energy

It is of special importance to estimate the anisotropy between the two horizontal motions (m.c. and angular velocity) and their dependence on the cycle phase. This will allow us to estimate how much energy is contained in small-scale eddies sampled by faculae, and the latitude-variation of this energy. Canuto et al. (1994) argued that large-scale effects (differential rotation, for example) could be generated by turbulence (i.e. small-scale effects) and that the small-scale motions might then contain more energy than the large-scale, contrary to what is usually assumed in most turbulence theories.

The term "turbulent kinetic energy" or "small-scale kinetic energy" leads us to discuss the important question of what the rms velocity represents precisely. We can decompose a velocity u (angular velocity or m.c.) into two components $u =< [u] > +u'$, where $< [u] >$ represents a large-scale mean (both spatially and temporally) and u' a motion fluctuation with a zero mean. We then define the turbulent kinetic energy as $\frac{1}{2}u'^2$. However, we measure u' at a given scale: in our case, the smallest scale we measure is the granulation scale (or slightly larger, for sunspots). Facula rms velocities contain various scales, from granulation to supergranulation or larger scales, so one has to be cautious when comparing observations to models.

5.1. Facula rms velocities

5.1.1. Contributions of instrumental rms velocities to observed rms velocities

The observed rms velocity V_{rms} (for rotation or m.c.) contains: 1- instrumental and tracking errors; 2- a hierarchy of scale contributions, from large-scale motions between faculae (i.e. analogous to the rms velocity observed for sunspots tracked using their barycenter) to small-scale motions (inside each facula, roughly at the scale of a few pixels). We are interested here in the rms velocity V_{rms} (V_{rms} is equal to $< [u'^2] >^{1/2}$) of the angular velocity v and of the m.c. u.

First we insist on the scattering due to measurement errors. A pixel represents a different surface area near the limb than it does at the disk center, and the corresponding scattering varies as

$$\sigma_u(\theta) = \frac{A}{\cos\theta}, \tag{1}$$

$$\sigma_v(\theta) = \frac{A}{\cos\theta\cos\phi} \sim \frac{A'}{\cos\theta}, \tag{2}$$

for u and v, respectively, where θ is the latitude, ϕ the disk longitude, and A and A' are small constant values in degrees/day. A' is pertinent if we are interested in the latitude-dependence with a longitudinal average. A' is a little higher than A by a factor about 1.15 in the [-50°,50°] in longitude domain. A and A' can be considered constant during the solar cycle, and are approximately of the order of one pixel (15 m/s).

5.1.2. Cycle 19 rms velocities

When subtracting polynomial fit $v(\theta)$ from individual angular velocities v_i, one can compute the angular rms velocities, $V_{\rm rms}$ being denoted as to $v_{\rm rms}$ in this case:

$$v_{rms} = \sqrt{\frac{\sum_{i=1}^{T}(v_i - v(\theta))^2}{T}}, \tag{3}$$

where T is the total number of points. The polynomial fit is performed using Legendre polynomials, and is described in Paper I. The m.c. rms velocities are computed by subtracting the averaged $\bar{u}_j$ in the latitude bin j from individual m.c. u_i, and is denoted $u_{\rm rms}$:

$$u_{rms} = \sqrt{\frac{\sum_{j=1}^{N}\sum_{i=1}^{N_j}(u_i - \bar{u}_j)^2}{T}}, \tag{4}$$

where N is the number of latitude bins and N_j the number of points in latitude bin j. The 1-σ error on the rms velocity V_{rms} is $V_{rms}/\sqrt{2T}$ (Parrat 1961).

We obtain for the whole facula data set [1957-1964]: v_{rms} = 0.491 ± 0.002°/day and u_{rms} = 0.352 ± 0.001°/day, or, in meters per second, v_{rms} = 65.51 ± 0.21 m/s and u_{rms} = 49.46 ± 0.16 m/s. Let us note for comparison that a typical horizontal velocity in supergranulation cells at the solar surface is 300 m/s, and, in granulation cells, of the order of 1 km/s. The facula anisotropy ratio v_{rms}/u_{rms} is 1.32±0.01.

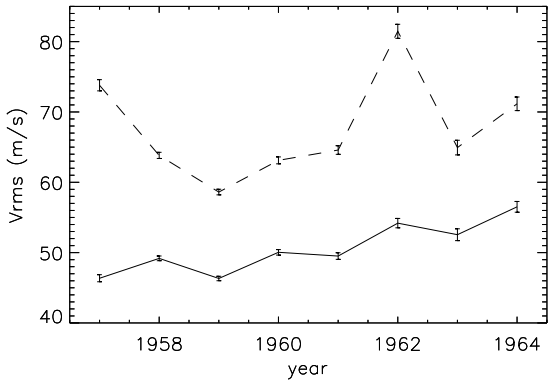

Fig. 5. u_{rms} (solid line) and v_{rms} (dashed line) for faculae in [1957-1964], in m/s

5.1.3. Variation of rms velocities

Fig. 5 shows the variation of facula rms velocities during cycle 19. The rms m.c. u_{rms} increases by a factor of some 1.2 (i.e. $\Delta u_{rms} \sim$10 m/s) from cycle maximum to minimum. The variation of the rms angular rotation v_{rms} is less clear, but it also seems to be smaller during cycle maximum (1959-1960) than at cycle minimum. The ratio v_{rms}/u_{rms} is maximum in 1957 (1.7) and then decreases from 1958 (1.4) to 1964 (1.3), except for 1962 (about 1.5). So we observe two major properties: the rms velocities increase from cycle maximum to minimum and the degree of anisotropy decreases.

These variations are significant at the level of several σ, especially for the m.c. Intrumental or tracking errors, as noted in Sect. 5.1.1, should be constant with time at a given latitude. However, their latitude-dependence (smaller errors at the equator), together with the equatorward migration of the magnetic activity, should lead to a decline of V_{rms} (for both u and v) when latitude-averaged. So the observed trend is strengthened. These observations are probably related to granulation or supergranulation property variations during the cycle. However, if they are related to angular rotation changes during the cycle, are these variations (-7 m/s) large enough? The decrease in anisotropy from cycle maximum to minimum could be produced by the decrease in the mean angular velocity.

5.2. Comparison with sunspot rms velocities

For the time-interval 1957 to 1962, sunspots exhibit v_{rms} = 77.52 $\pm$ 1.12 m/s and u_{rms} = 38.73 $\pm$ 0.56 m/s. The rms angular velocity is thus higher for sunspots than for faculae (ratio 1.18) but the rms m.c. is lower (ratio 0.78). Thus the ratio v_{rms}/u_{rms} is higher for sunspots (2.00$\pm$0.04) than for faculae (1.32). The difference between these facula and sunspot rms velocities could be due to the anchorage depth of sunspots, faculae being more sensitive to surface effects. Facula rms velocity also contains a greater contribution from small-scale effects than that of sunspots, because we are tracking facular points. These small-scale features probably have more isotropic properties, i.e. they are less sensitive to the preferential direction of angular rotation, because of their higher Rossby number. A large anisotropy present in sunspots could then be due to large-scale effects. Sunspots V_{rms} show no significant variations during the cycle.

Let us recall that we observed in Paper I a shape-asymmetry in the sunspot rotation rate distribution. This shape-asymmetry was interpreted in terms of two populations (of smaller width). So the sunspot v_{rms} due to small-scale effects might be smaller than the one measured.

5.3. Latitude-dependence of the small-scale kinetic energy

The rms velocity computed in the previous subsections can be interpreted as a "turbulent" (or "small-scale") kinetic energy. If dispersion is mainly of solar origin and due to small-scale motions, this should yield to important information about the latitudinal-dependence of the small-scale kinetic energy and its amplitude.

We compute the "turbulent kinetic energy" (i.e. energy associated with velocity fluctuations) as

$$E_{kin} = \frac{1}{2} V_{rms}^2, \tag{5}$$

for both v and u, where V_{rms} is defined in Eqs. 3 and 4. The error in E_{kin} is derived from the error on the rms velocity, and is

$$\sigma_{Ekin} = E_{kin} \sqrt{\frac{2}{T}}, \tag{6}$$

where T is the number of points. It is pertinent to calculate E_{kin} values versus latitude, in order to compare them with numerical models. Fig. 6 shows these values for both faculae and sunspots.

The turbulent kinetic energy associated with facula m.c. is approximately constant with latitude. The latitude-dependence is stronger for the angular rotation, but is also noisier. We observe in general an increase in E_{kin} with latitude by a factor two. However, this trend nearly disappears when expressed in $(m/s)^2$.

The E_{kin} associated with sunspot angular velocity shows larger amplitude variations than the E_{kin} of the m.c obtained with the same sunspots. The angular velocity E_{kin} is minimum at the equator and at 40°N. A large peak is present at 15°S in the southern hemisphere. The E_{kin} of m.c. is similar to those for faculae.

5.4. Comparison with models

We found a nearly constant energy contribution of small-scale motions, in qualitative disagreement with the algebraic model of Canuto et al. (1994). These authors predicted a strong latitude-dependence: a peak at a latitude of about 35° with an amplitude roughly twice that of the equator. If we keep in mind that the error measurements in our data increase with latitude, the discrepancy with the prediction of Canuto et al. is even greater.

The amplitude of $E_{kin}/e_\star$, where $e_\star$ is a typical turbulent kinetic energy, is smaller than the model of Canuto et al. by a

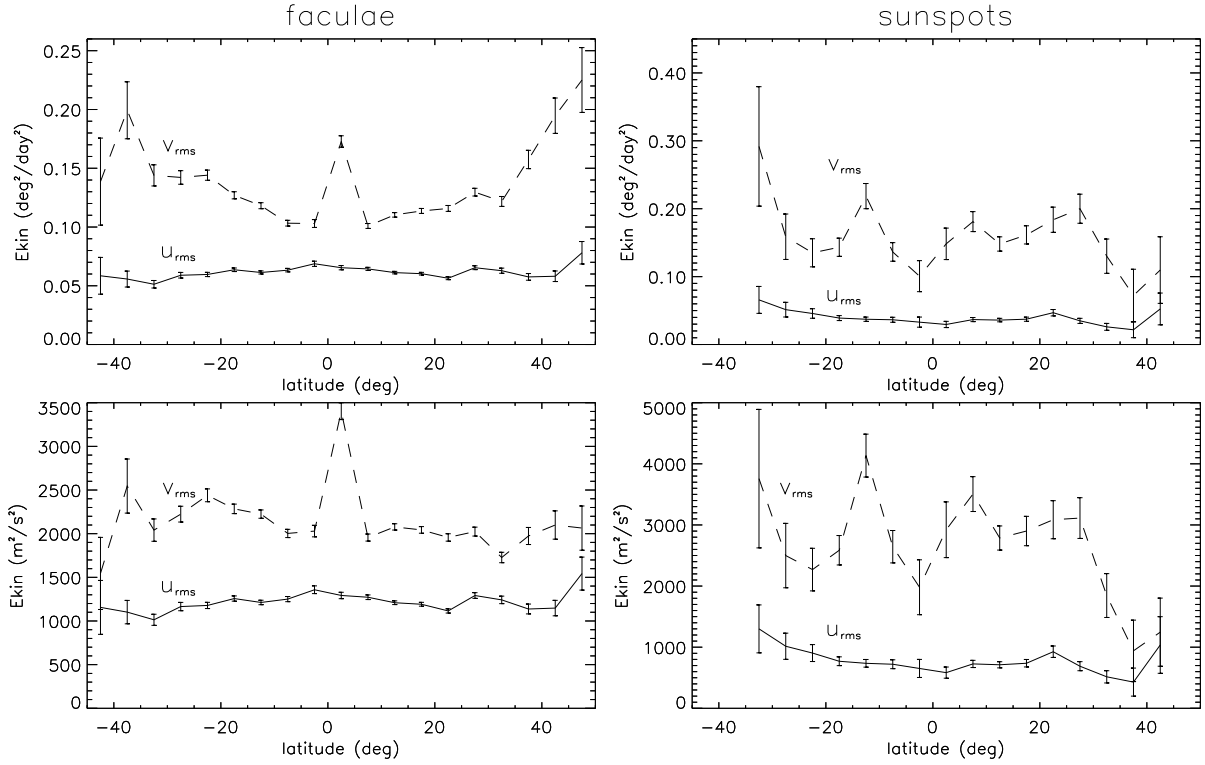

Fig. 6. Turbulent kinetic energy versus latitude for faculae (left) and sunspots (right). The two figures at the top are given in $(^\circ/\mathrm{day})^2$, and the two at the bottom are given in $(\mathrm{m/s})^2$. The solid lines correspond to $u_{rms}(\theta)$ and the dashed lines to $v_{rms}(\theta)$, where θ is the latitude

factor about 2 for faculae, and a little less for sunspots. So we suggest that small-scale eddies may not contain as much energy as assumed by Canuto et al.

However, the discrepancy between our observations and the model is certainly a problem of selected motion scales. In the algebraic model of Canuto et al., the typical scale is smaller than the smallest observed scale here. For example, it is smaller than the granulation size. On the other hand, in numerical models, the velocity fluctuations u' correspond to the mesh size, e.g. 30000 km in the recent model of Pulkkinen et al. (1993).

Therefore, comparison between observations and models are not straightforward. In the case of a Kolmogorov turbulence, the rms velocity varies as $l^{1/3}$, where l is the typical scale. So the fluctuation amplitudes of u' and E_{kin} depend in a complex way on the scale at which they are measured.

Moreover, we observed a hierarchy of scales, from the granule scale (1000 km) to the supergranule scale (30000 km). Each scale possibly depends on latitude and depth. For example, supergranulation cell size are observed to decrease with increasing latitude (Brune & Wöhl 1982; Rimmele & Schröter 1989; Münzer et al. 1989); the model of Pulkkinen et al. exhibits a radial-averaged turbulent kinetic energy, but these authors mentioned that great variations with depth have been observed.

If compared with the radial average, the turbulent kinetic energy we found exhibits a latitude-dependence similar to the model of Pulkkinen et al. (1993), which does not show a strong peak around 30°.

6. Covariance and angular momentum transport

We now address the important question of the angular momentum transport, which is related to the generation of the Sun's differential rotation. We estimate the transport by the m.c. (axisymmetric term) and by Reynolds stresses (non-axisymmetric term), which result from the interaction between non-axisymmetric motions and the Coriolis force. Reynolds stresses are represented by the correlation between motions in the two horizontal directions (i.e. the "covariance"). Most current models favor this process.

In this section, meridional motion is positive when towards the equator and negative when towards the pole, in both hemispheres. Previous studies (Ward 1965) showed that the linear angular momentum transport across a complete latitude circle of length L over the time t is

$$\tau \cong tL\rho < [uv] >, \tag{7}$$

where ρ is an average density. Then τ is proportional to

$$< [uv] >=< [u] >< [v] > + < [u]^*[v]^* > + < [u^\bullet v^\bullet] >, \tag{8}$$

where [ ] indicate spatial averages, $< >$ time averages, $u^\bullet$ and $v^\bullet$ are spatial deviations for each day of the period, and $[u]^*$ and $[v]^*$ are time deviations. The first term, $< [u] >< [v] >$, represents the transport by meridional motion (hereafter "M.C.T."). The two last terms correspond to transports by fluctuating cells (time-variable eddy transport) and horizontal eddies (space-variable eddy transport), respectively. In our analysis, these two

terms cannot be separated because there are not enough points within each latitude bin for each image pair. But the sum of the two terms can be computed, using the space and time-averages of u and v. This sum is referred to as the covariance between the motions in the two horizontal directions, and is expressed by

$$< [u'v'] >=< [(u- < [u] >)(v- < [v] >)] >, \quad (9)$$

where u' and v' are the deviations from the respectively time and space means (in each latitude bin) $< [u] >$ and $< [v] >$ (Nesme-Ribes et al. 1993b). With our sign convention, a positive covariance means that motion faster than average in the direction of rotation is coupled with equatorward motion. The covariance represents the angular momentum transport by Reynolds stresses.

6.1. Latitudinal dependence

The M.C.T. across the latitude circle corresponding to latitude bin i is

$$\text{M.C.T.}_i = \bar{u}_i\bar{v}_i, \quad (10)$$

where $\bar{u}_i$ and $\bar{v}_i$ are the average of u and v in latitude bin i. The 1-σ error on the M.C.T. includes the standard errors on $\bar{u}_i$ and $\bar{v}_i$. The covariance in the latitude bin i is

$$< [u'v'] >_i = \frac{\sum_{k=1}^{N_i}(u_k - \bar{u}_i)(v_k - \bar{v}_i)}{N_i}, \quad (11)$$

where N_i is the number of points within a given bin i. The 1-σ error on the covariance has two contributions: the dispersion in the latitude bin and the error on $\bar{u}_i$ and $\bar{v}_i$. The main contribution comes from the latter for both the M.C.T. and the covariance. This is due to the high uncertainty in m.c., especially in the southern hemisphere.

6.1.1. Latitudinal-dependence of facula covariance

Fig. 7 shows the angular momentum transport by Reynolds stresses (covariance) and by m.c. (M.C.T.). The two hemispheres are folded symmetrically about the equator. We observe no significant covariance, and the error bars provide an upper limit. For faculae, we get covariance values smaller than 0.002 ($^\circ$/day)^2 for most latitude bins (remembering that there are fewer points at high latitudes) and an upper limit of 0.01 ($^\circ$/day)^2 at the 1-σ confidence level. Fig. 8 presents the same curves for the two hemispheres, separately. The covariance is still very small (below the 1-σ error bars).

This is in disagreement with results by Schröter & Wöhl (1976), who studied proper motions of Ca^+-network fine mottles, as shown by Table 2, and by Belvedere et al. (1976). The values given by these authors correspond to latitude-averaged covariance because they were not looking for latitudinal-dependence. However, Komm et al. (1994), observing small-scale photospheric magnetic fields (from magnetograms), did not detect any significant covariance when considering the latitudinal dependence.

Küker et al. (1993) predicted a covariance which is positive near the surface and negative at the bottom of the convective zone. Their amplitude is probably no greater than a few 0.01 ($^\circ$/day)^2, but it is depth-dependent, especially near the surface. So this recent model is consistent with our observations.

6.1.2. Latitudinal-dependence of facula M.C.T.

Facula M.C.T. (defined by Eq. 10) is poleward in the northern hemisphere and less significant in the southern hemisphere; this was already noticed in Fig. 1. We note that a poleward M.C.T. (related to the poleward m.c.) implies that there is some depth at which there should be an equatorward m.c., for continuity. The surface poleward M.C.T. is associated with global transport of angular momentum towards the pole, only if there is enough diffusion to couple the different layers. Otherwise, deep layers would transport the same momentum towards the equator and the balance would be null (Gilman 1980). So it is difficult to estimate the total M.C.T. (i.e. over the whole convective zone) from the surface estimation only. The M.C.T. we measure is only the transport contribution of a layer at a given depth.

6.1.3. Comparison with sunspots

Figs. 7 and 8 also display the covariance and M.C.T. for sunspots versus latitude (Nesme-Ribes et al. 1996b). Sunspot covariance is less than 0.02 ($^\circ$/day)^2, with an upper limit at the 1-σ level of 0.05 ($^\circ$/day)^2, which is rather similar to facula covariance. This covariance is much smaller than other observations of sunspot groups (Ward 1965) and sunspots (Gilman & Howard 1984), as shown in Table 2. But our results confirm the small covariance found by Nesme-Ribes et al. (1993b) for cycle 21 sunspots.

Sunspots exhibit an equatorward transport at low latitudes ($< 20^\circ$) and poleward above those latitudes, which is significant at the 1-σ level only because the errors are large. The difference between sunspot and facula covariance probably lies in the magnetic field strength and anchorage depth of these magnetic features.

6.2. Total contribution for each hemisphere

The above covariance was calculated for each 5° latitude bin: the linear angular momentum was defined across a latitude circle of length L. The covariance obtained was not significantly different from zero for both faculae and sunspots, and we could not obtain their latitudinal-dependence either. In this section we compare each hemisphere. Let us note that the results of Belvedere et al. (1976) are available only for the whole surface. The total M.C.T. is estimated as

$$\text{M.C.T.} = \frac{\sum_{i=1}^{N} N_i \cos\theta_i \bar{u}_i\bar{v}_i}{\sum_{i=1}^{N} N_i}, \quad (12)$$

where N_i is the number of points in the latitude bin i, N the number of latitude bins, and θ_i the mean latitude of the bin.

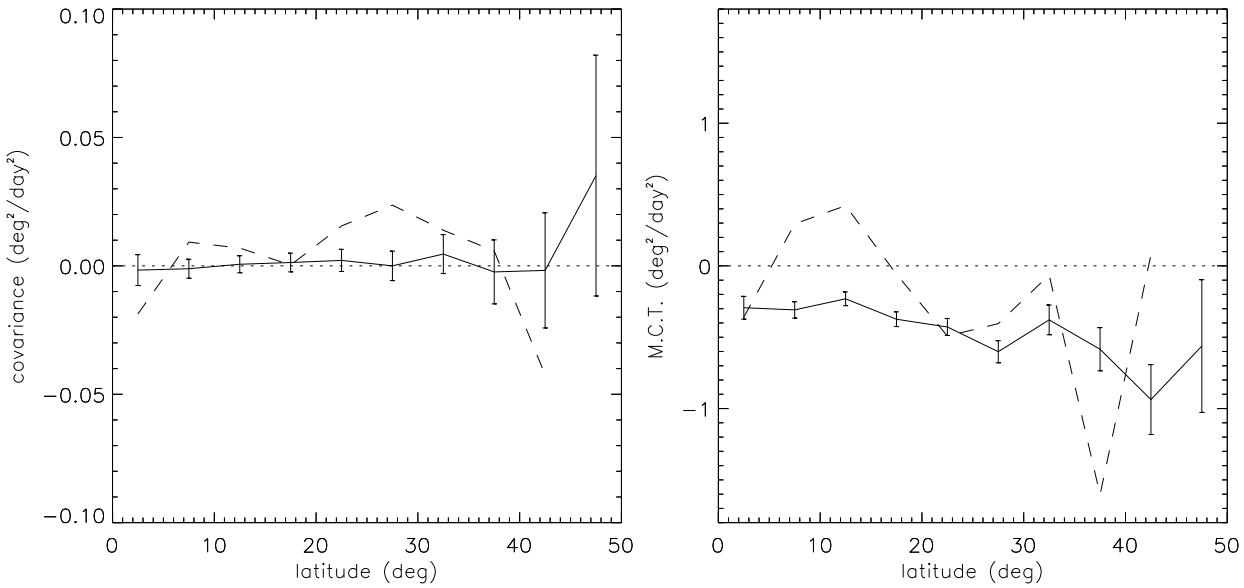

Fig. 7. Angular momentum transport by Reynolds stresses (covariance) are shown on the left and by meridional motions (M.C.T.) on the right. Solid lines represent faculae during [1957-1964] and dashed lines sunspots during [1957-1962]. The two hemispheres have been folded. The values are given in $(^\circ/\mathrm{day})^2$. Error bars for sunspots are not plotted, to make the reading easier. For the covariance the error has the same order of magnitude as the signal. For the M.C.T., the signal is slightly above the error bars

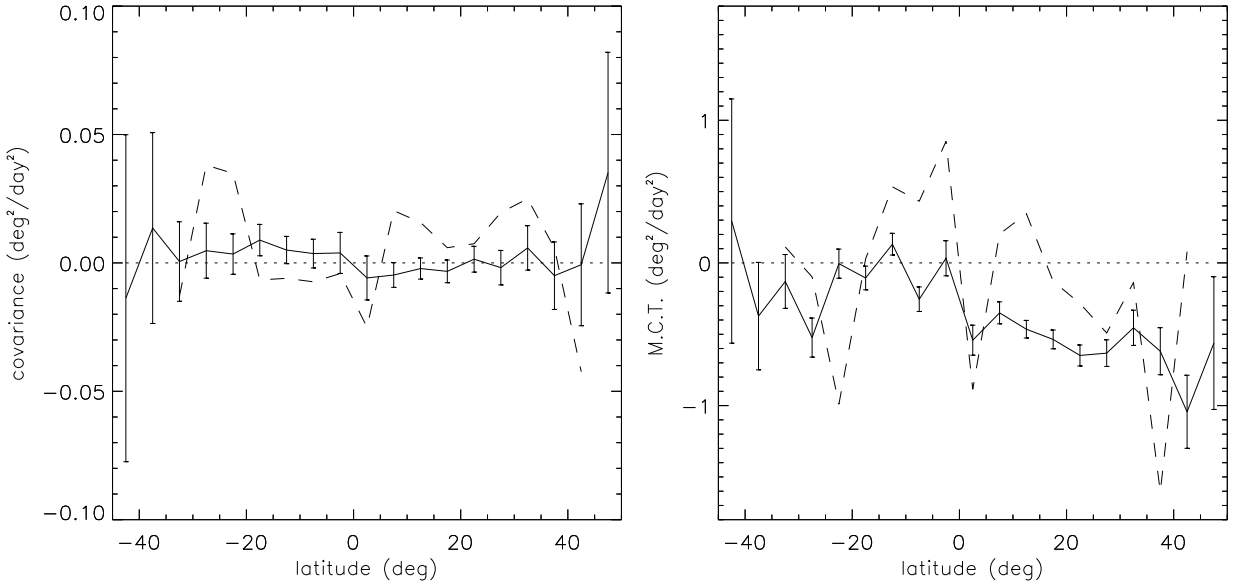

Fig. 8. Same as Fig. 7, except that the two hemispheres are unfolded

Table 2. Covariance values found by various authors using different tracers

authors	tracers	covariance $(^\circ/\mathrm{day})^2$
Schröter & Wöhl 1976	Ca^+-network fine mottles	0.2
Belvedere et al. 1976	K faculae (barycenter)	0.05 to 0.2
Komm et al. 1994	small-scale magnetic fields	0.01 (monthly averaged value)
present paper	photospheric faculae (cycle 19)	0.002 (max. 1-σ: 0.01)
Gilman & Howard 1984	sunspots	0.08 (max., latitude=30°)
Ward 1965	sunspot groups	0.15 (max., latitude=30°)
Nesme-Ribes et al. 1993b	sunspots (cycle 21)	0.02
Nesme-Ribes et al. 1996b	sunspots (cycle 19)	0.02 (max. 1-σ: 0.05)

Table 3. Covariance and M.C.T. for the whole cycle faculae (1957 to 1964) and sunspots (1957 to 1962) averaged on latitudes (North, South, all latitudes), in $(^\circ/\mathrm{day})^2$

	faculae	sunspots
covariance North	-0.0008 $\pm$ 0.0017	0.0112 $\pm$ 0.0045
covariance South	0.0060 $\pm$ 0.0021	-0.0007 $\pm$ 0.0053
covariance all	0.0008 $\pm$ 0.0011	0.0068 $\pm$ 0.0036
M.C.T. North	-0.516 $\pm$ 0.076	-0.038 $\pm$ 0.128
M.C.T. South	-0.066 $\pm$ 0.054	0.208 $\pm$ 0.169
M.C.T. all	-0.321 $\pm$ 0.048	0.054 $\pm$ 0.105

The weighting of the transport in each latitude bin by $\cos\theta_i$ is introduced to take into account the L-dependence of τ, but this does not strongly influence the results. The 1-σ error on the M.C.T. includes the dispersion between latitude bins and the standard errors on $\bar{u}_i$ and $\bar{v}_i$. The covariance is

$$< [u'v'] >= \frac{\sum_{i=1}^{N} \cos\theta_i \sum_{k=1}^{N_i} (u_k - \bar{u}_i)(v_k - \bar{v}_i)}{\sum_{i=1}^{N} N_i}. \qquad (13)$$

The 1-σ error on the covariance now has three contributions: the dispersion between latitude bins, the dispersion in each latitude bin, and the errors on $\bar{u}_i$ and $\bar{v}_i$.

Table 3 shows the covariance and the M.C.T. when averaged in time (over the cycle) and over the latitudes (for all latitudes, and each hemisphere, separately). The covariance is still very small and not very significant, except for southern faculae (but the corresponding m.c. was not very significant) and for northern sunspots. The covariance for all facular points (averaged in time and latitude) is $6\,10^4 \pm 2\,10^5 (\mathrm{cm/s})^2$, i.e. smaller than $6\,10^5$ $(\mathrm{cm/s})^2$ at the 3-σ confidence level. This is one to two orders of magnitude smaller than those given by Belvedere et al. (1976): they found covariance values ranging from 10^7 to $4\,10^7$ $(\mathrm{cm/s})^2$ depending on facula size and compactness. However, they did not give any error bar on their values. Schröter & Wöhl (1976) also found a value of $4\ 10^7$ $(\mathrm{cm/s})^2$ for Ca^+-network fine mottles.

The transport by the m.c. is much higher (several orders of magnitude) and always negative (i.e. poleward) for faculae. Results for sunspots are less significant, but there is an equatorward M.C.T. in the southern hemisphere.

6.3. Time dependence of the angular momentum transport

In the previous section, we showed that the cycle- and latitude-averaged covariance was not significant. So we now study the time-variation of the latitude-averaged covariance when averaged yearly. The covariance could become significant over times shorter than the solar cycle. Fig. 9 shows the variation of the covariance and the M.C.T. for faculae during cycle 19, computed for the northern and the southern hemispheres separately. We observe a roughly positive covariance in the South, and negative in the North. This confirms Table 3. So covariance is more significant on shorter periods (1 year). This has been observed by Komm et al. (1994), but at a different scale: they found their most significant covariance at a 1 month-scale, while yearly covariance was insignificant. They obtained a covariance smaller than 0.01 $(^\circ/\mathrm{day})^2$, i.e. similar to ours. This is not surprising if we recall that facular points can be associated with small-scale magnetic fields.

In the northern hemisphere, M.C.T. is negative and |M.C.T.| is higher at cycle maximum: M.C.T. would reinforce the rigidity of the rotation at cycle maximum.

Covariances in each hemisphere also seem to be in antiphase. The correlation factor between the two hemispheres is -0.25. This is also true for the M.C.T., with a correlation factor of -0.50. Even though the signal in the southern hemisphere is close to zero, the two hemispheres are strongly anticorrelated, with variations having a typical time-scale of the order of a few years. This could characterize exchanges between the two hemispheres, especially via the interactions at the equator, implying an active role of the large-scale motions.

7. Conclusion

We used different approaches to address the question of facula dynamics. We first observed a strong north-south asymmetry of the facula m.c., with poleward motions up to 7 m/s in the northern hemisphere at cycle maximum, and no significant m.c. in the southern hemisphere.

The m.c. histogram confirms and states with greater precision what has been discovered in Paper I: we detected a facula population, containing about 10% of the data set points, that rotated more slowly than average, showing m.c. around ten times smaller than the mean, and with rms velocities in the two directions (east-west and north-south) ten times smaller than the rms velocities for the whole data set. Polar field reversals are consistent with the m.c. north-south asymmetry.

Observations of facula and sunspot rms velocities, and their variation during the cycle, allowed us to detect their anisotropy and the origin of their dispersion more precisely. The action of convective cells on facular points or on sunspots maybe due to the cells' horizontal motions and to the successive emergences and disappearances of cells.

Let us note first that a 50 m/s velocity (typical rms velocity for faculae and sunspots) corresponds to a daily displacement equivalent to the size of three granules, while a granule has a typical lifetime of only five minutes. We found no observation of the dependence of the granular or supergranular horizontal velocities on the cycle-phase. Convective cell sizes have been more widely studied. Granules are smaller at cycle maximum (Muller 1988; Muller et al. 1989) and near active regions, as observed by Macris et al. (1989), who found a factor of some 1.15 between the granule size in active and quiet regions. This is consistent with our observations if the mechanism of granule emergence/disappearance prevails.

On the other hand, Münzer et al. (1989) showed that supergranulation cells were larger near active centers. These last observations are in disagreement with our observations if supergranule emergences/disappearances play a significant role, because at the end of the cycle there are fewer very active regions

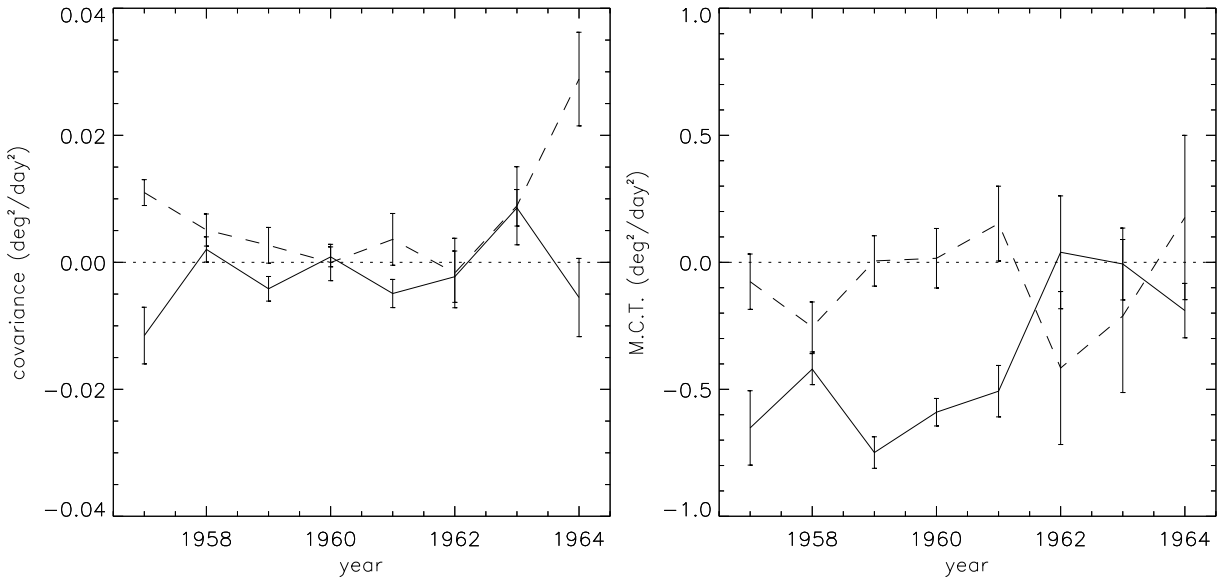

Fig. 9. Variation of the angular momentum transport by Reynolds stresses (covariance) during the cycle is shown on the left and by meridional motions (M.C.T.) on the right, for faculae. The northern hemisphere is shown in solid lines and the southern in dashed lines. Values are given in $(^\circ/\mathrm{day})^2$

than at its maximum, so a larger proportion of points belongs to regions of small activity (i.e. larger granules but smaller supergranules).

This suggests that granulation plays a preponderant role in the rms velocities of facular points via their emergence/disappearance, while supergranulations probably influences motions via their horizontal velocities. The observed discrepancies may be due to the radial structures of the cells.

At a larger scale (about 20°), Nesme-Ribes & Mangeney (1992) found that kinetic energy associated with m.c. bands was higher at cycle minimum than at maximum. This is also consistent with our observations. However, faculae did not show any well-defined m.c. pattern, in contrast with sunspots. This is an important point to stress, because faculae rms velocities should also contain a large-scale contribution.

The crude turbulent kinetic energy calculated in the present paper does not reveal any strong latitudinal-dependence, though this dependence is difficult to determine. Our estimate is probably smaller (by a factor of at least two) than the value predicted by Canuto et al. (1994). The discrepancy between observations and model might be due to a scaling effect.

Facula covariances averaged over the whole cycle are hardly significant, while yearly values are negative for the North. Their amplitude is smaller than 0.01 $(^\circ/\mathrm{day})^2$, which is consistent with the results of Komm et al. (1994) for small-scale magnetic fields. Sunspots also exhibit a small covariance, in agreement with cycle 21 Meudon sunspots (Nesme-Ribes et al. 1993b).

Most theoretical studies seem to favor large covariance rates (Canuto et al. 1994; Pulkkinen et al. 1993). However, the small facula covariance does not bring into question the role of Reynolds stresses in the equatorial acceleration. Covariance is likely to be depth-dependent, as shown by Küker et al. (1993). A precise knowledge of the anchorage depth of magnetic tracers is crucial to settling the issue of the origin of solar differential rotation.

Acknowledgements. One of us (E. Nesme) is grateful to the Ministery of Defense, for having encouraged and funded the long-term spectroheliogram research program, through military contracts (no. 010481/ETCA, no. 012736/DRET-ETCA, and no. 92-2011.A/DRET-ETCA). The extensive work of the spectroheliogram observations team has been crucial for almost a century. We thank the present team for maintaining and improving the observational program over the years. Spectroheliograms were digitized with the *Machine à Mesurer pour l'Astronomie* (MAMA) of the Institut National des Sciences de l'Univers, at the Paris Observatory. Our thanks also go to P. Micheneau, R. Chesnel, P. Toupet, and M. Savinelli for their assistance in the data acquisition and processing.

References

Babcock H.D., 1959, ApJ 130, 364
Belvedere G., Godoli G., Motta S., Paternò L. & Zappalà R.A., 1976, Sol. Phys. 46, 23
Brune R. & Wöhl H., 1982, Sol. Phys. 75, 75
Canuto V.M., Minotti F.O. & Schilling O., 1994, ApJ 425, 303
Choudhuri A.R., Schüssler M. & Dikpati M., 1995, A&A 303, L29
Collin B., Nesme-Ribes E., Leroy B., Meunier N. & Sokoloff D., 1995, C. R. Acad. Sci., Paris, t.321, Série IIb, 111
Gilman P.A. & Howard R.F., 1984, Sol. Phys. 93, 171
Gilman P.A., 1980, in: Stellar Turbulence, Lecture Notes in Physics 114, D.F. Gray & J.L. Linsky eds., 19
Godoli G., 1969, Sol. Phys. 9, 246
Komm R.W., Howard R.F. & Harvey J.W., 1993, Sol. Phys. 147, 207
Komm R.W., Howard R.F. & Harvey J.W., 1994, Sol. Phys. 151, 15
Küker M., Rüdiger G. & Kitchatinov L.L., 1993, A&A 279, L1

Leighton R.B., 1969, ApJ 156, 1
Macris C., Prokakis Th., Dialetis D. & Muller R., 1989, Sol. Phys. 122, 209
Makarov V.I., 1984, Sol. Phys. 93, 393
Meunier N., Nesme-Ribes E. & Grosso N., 1996, accepted in A&A (Paper I)
Muller R., 1988, Advances in Space Research 8 no. 7, 159
Muller R., Hulot J.C. & Roudier T., 1989, Sol. Phys. 119, 220
Münzer H., Hanslmeier A., Schröter E.H. & Wöhl H., 1989, A&A 213, 431
Nesme-Ribes E. & Mangeney A., 1992, Radiocarbon 34 n° 2, 263
Nesme-Ribes E., Ferreira E.N. & Mein P., 1993a, A&A 274, 563
Nesme-Ribes E., Ferreira E.N. & Vince I., 1993b, A&A 276, 211
Nesme-Ribes E., Meunier N. & Collin B., 1996a, A&A 308, 213
Nesme-Ribes E., Meunier N. & Vince I., 1996b, accepted in A&A
Parrat L.G., Probability and experimental errors in science, eds. Dover, 1961
Pulkkinen P., Tuominen I., Brandenburg A., Nordlund A. & Stein R., 1993, A&A 267, 265
Ribes E. & Bonnefond F., 1990, Geophys. Astrophys. Fluid Dynamics 55, 241
Rimmele T. & Schröter E.H., 1989, A&A 221, 137
Rüdiger G., 1977, Astron. Nachr. 298, 245
Rüdiger G. & Kitchatinov L.L., 1994, in: NATO ASI Series I, vol 25, E. Nesme-Ribes ed., 27
Schröter E.H. & Wöhl H., 1976, Sol. Phys. 49, 19
Sheeley N.R.Jr., 1976, J. Geophys. Res. 81(19), 3462
Stix M., 1989, Reviews in Modern Astronomy 2, 248
Ward F., 1965, ApJ 141, 534

This article was processed by the author using Springer-Verlag LaTeX A&A style file *L-AA* version 3.